Transportation Research Part D 122 (2023) 103807

Contents lists available at ScienceDirect

Transportation Research Part D

journal homepage: www.elsevier.com/locate/trd

Integrated infrastructure planning of charging and electricity generation

Xiasen Wang [a], Jiwan Jiang [b], Yang Zhou [c], Xin Wang [d,*]

[a] Sustainable Transportation Lab, University of Washington, Seattle, WA 98105, USA
[b] Department of Civil and Environmental Engineering, University of Wisconsin-Madison, Madison, WI 53706, USA
[c] Zachry Department of Civil and Environmental Engineering, Texas A&M University, College Station, TX 77840, USA
[d] Department of Industrial and Systems Engineering, University of Wisconsin-Madison, Madison, WI 53706, USA

ARTICLE INFO

Keywords:
Facility location
Traffic assignment
Wireless charging lane
Bi-level optimization

ABSTRACT

With the rapid development of charging-while-driving technology, the deployments of wireless charging lanes will inevitably affect the route choice of Battery Electric Vehicle (BEV) drivers and the power supply of power grids. This paper builds a bi-level optimization problem to optimize the locations of charging lanes and charging stations given an integrated transportation-power network. The decision variables of the upper level include the locations of charging lanes and charging stations and the electricity generated in each busbar (an electricity generation node in the power network), while the lower level determines the charging strategy and the route choice of the drivers. Then we develop an effective solving algorithm for the problem through various reformulations. The results from the numerical study and sensitivity analysis show that charging infrastructures' deployment affects the route choices of BEV drivers significantly, and charging lanes can be a more economical and effective charging method than charging stations.

1. Introduction

Battery electric vehicles (BEVs) are believed to reduce air pollution and fossil fuel dependence (Duvall et al., 2004; He et al., 2022). However, one critical limitation of its large adoption is the shortage of charging infrastructures compared with gas-fueled vehicles (Maitra et al., 2010). Recently, with the improvement of battery technology and charging facilities, a massive increase in BEV adoption is expected (Kapustin and Grushevenko, 2020). As indicated by Narassimhan and Johnson (2018), early investments in charging infrastructures, especially along highways, play a significant role in increasing BEV adoption in the US according to the BEV purchase data from 2008–2016. Meanwhile, many countries have developed incentive programs to deploy public electric vehicle charging infrastructure in place (Adenaw and Krapf, 2022).

Public charging infrastructures for BEVs consist of various types of facilities. Among them, Level 2 (L2) chargers (Funke et al., 2019) are commonly used in private homes or public parking lots. However, the charging rate of L2 chargers is relatively slow, requiring long parking times, often overnight, to fully recharge a BEV. This causes the well-known range anxiety (Bonges III and Lusk, 2016), which significantly limits the adoption of BEVs for long-distance travel. To mitigate this issue, direct current fast chargers (DCFCs) have been developed. DCFCs can charge passenger cars at up to 500 V and can charge most BEVs to 80% state-of-charge (SOC) within 30 min (Longo et al., 2016). However, this charging time is still much longer than the refueling time for traditional

* Corresponding author.
E-mail address: xin.wang@wisc.edu (X. Wang).

https://doi.org/10.1016/j.trd.2023.103807
Received 7 October 2022; Received in revised form 2 May 2023; Accepted 5 June 2023
Available online 22 August 2023

gasoline vehicles, which may significantly limit the efficiency of BEV travel without sufficient charger networks, especially when travel demand surges. This can result in critical vulnerability of the transportation network.

In order to further address the issue of charging time bottleneck, the development of dynamic charging lanes has been envisioned as a potential solution, particularly in light of the increasing adoption of battery electric vehicles (BEVs). There are two primary technologies utilized in the construction of charging lane: the conductive method and the inductive method. The former employs overhead electric wires or metal bars on the pavement to transmit electric power to the vehicles, while the latter employs a range of waves (such as laser, photoelectric, radio waves, microwaves, and magnetic resonance coupling) to transfer electricity to vehicles without the need for physical connections (Lukic and Pantic, 2013). Within the context of our discussion, we focus on the inductive method due to its convenience and flexibility in relation to private cars. The implementation of dynamic charging lanes will result in two significant enhancements for long-distance BEV travel. First, the BEV travel time will not be significantly affected by the need to recharge, as they will be able to both drive and charge simultaneously. This eliminates the need for BEVs to stop at charging stations and wait in line, thereby streamlining the overall travel process. Second, the capacity of charging lanes is designed to accommodate mass BEV charging concurrently. The charging capacity will be the same as the road capacity, hence there is no waiting for charging once the charging lane is used.

Despite the various attractive features of dynamic charging lanes, their implementation brings more challenges to the network design compared to the DCFC station decisions. First, the charging lane requires much higher initial infrastructure investment. Besides, the charging demand fluctuations associated with these lanes can have a considerable impact on power grid operations. Unlike DCFC stations, which are typically managed by local distribution power networks, charging lanes may require the cooperation of multiple power generators over long-distance transmission lines through the power grid network. This complicates the power network management, which needs to be coordinated with the BEV demand distribution. Specifically, the charging and routing choices of BEV drivers can affect the operational status as well as the background power grid cost and balance. Moreover, the charging availability also influences the route and charging strategy of BEV drivers.

Both charging stations and charging lanes have their own advantages and disadvantages. Charging stations provide convenience and relatively low installation costs, but causing disruptions due to long charging times, while charging lanes provide a more seamless charging experience, but come with higher installation costs. Given such trade-off, a combination of both charging methods is valuable to serve a wide range of BEV demand pattern (Chen et al., 2018).

In light of this, this paper aims to develop an optimal strategy for jointly deploying charging stations and charging lanes, considering their mutual impact on the power grid. We stand at the angle of a government agency which coordinates both transportation and energy sectors, considering each BEV driver's decision. The problem is formulated as a Stackelberg leader–follower game, with the upper level objective being to minimize the sum of total travel cost and the power generation cost, and the lower level captures the route choice decisions of each BEV driver, taking into account traffic congestion and charging availability, to form a traffic equilibrium. Specifically, we develop a holistic bilevel network optimization model that covers both the planning and operating stages. The upper level provides charging infrastructure deployment decisions including the locations of charging lanes and the DCFC stations. Given these upper-level decisions, the lower level captures the behavior of BEV drivers whose route choices minimize the travel time, considering charging duration. In the lower level, all BEV drivers form a traffic equilibrium, which determines the total transportation cost and electricity generation cost as feedback to the upper-level problem. Such bilevel optimization is a well-known non-convex, game-theoretical model is challenging to solve, hence an efficient algorithm is developed by converting it into a single level mix-integer linear programming problem, which is solved using commercial solvers. A numerical simulation is conducted to validate the efficiency of our model and provide interesting managerial insights.

This paper is organized as follows. In Section 2, a literature review is provided to summarize previous research on charging infrastructure deployment for BEVs. Section 3 establishes the bilevel optimization framework for our problem. Section 4 discusses the solution method based on linearization and mixed-integer reformulation. Section 5 presents numerical and sensitivity analyses to visualize the infrastructure deployment and its corresponding traffic equilibrium. Finally, Section 6 concludes the paper with a summary of our findings and directions for future research.

2. Literature review

The planning decision in our work is an extension of the charging station deployment decision problem. Numerous methods have been proposed to determine the location of DCFC charging stations, which have been reviewed comprehensively by Kchaou-Boujelben (2021). Early attempts to solve the charging/fueling station location problem include greedy heuristics proposed by Berman et al. (1992) and Hodgson et al. (1996), which produced good quality results within short computation times. Meta-heuristic methods, such as genetic algorithms, have been developed by many researchers to solve the charging station location problem, including Dong et al. (2014), He et al. (2015), Kang et al. (2015), Xie et al. (2018), and Kadri et al. (2020). When the problem objective involves non-linear components, good approximation algorithms are needed to overcome computational difficulties. For instance, Wu and Sioshansi (2017) developed an approximation strategy to locate EV charging stations when EV flow is uncertain, and Zhang et al. (2016) employed piecewise linearization to reformulate the location problem of DCFC while considering both the power distribution network and transportation network. Another challenge in locating charging stations is to consider the driving behavior of BEV drivers. He et al. (2015) established a bilevel modeling structure to deploy DCFCs while considering BEV drivers' route choice decision due to traffic congestion. However, as we have mentioned, deploying only DCFC stations may not meet the huge demands of BEV drivers, especially during long-distance travel under a large BEV adoption rate.

Unlike charging stations, the deployment of charging lanes has received limited attention in the literature due to its nascent stage of development. Tan et al. (2022) provided an overview of the existing studies on charging lanes and highlighted the need for more flexible and dynamic design and allocation models. Jang (2018) categorized the allocation problem of charging lanes into micro-allocation and macro-allocation models. The micro-allocation models aim to optimize the locations and lengths of charging lanes over a few paths. For instance, the On-Line Electric Vehicle (OLEV) system, which is a charging lane bus-transit system currently operational in Korea, represents a typical micro-allocation scenario. Various studies have focused on the allocation model of OLEV, such as those for bus routes (Jang et al., 2015; Jeong et al., 2015; Ko et al., 2015; Jang et al., 2016). In contrast, this paper concentrates on the macro-allocation scope of charging lanes.

Several studies have addressed the allocation problem of charging lanes, although not all of them have taken into account the route choice of BEV drivers. Wang et al. (2019) focused on the deployment of charging lanes considering the influence of traffic lights. Similarly, Mubarak et al. (2021) considered the power capacities of charging lanes in the transportation network, but they did not consider the impact of the allocation problem on the traffic conditions. On the other hand, some studies have considered route choices in the allocation problem. For instance, Chen et al. (2016) employed traffic equilibrium to assign BEVs to the transportation network and determine the optimal locations of the charging lanes. He et al. (2020) proposed an optimal deployment model for charging lanes, taking into account their effects on drivers' route choices and road capacity. Additionally, Ngo et al. (2020) proposed a bilevel deployment model that minimizes emissions on the upper level while the lower level is set to satisfy the traffic equilibrium conditions.

However, to the best of our knowledge, very few researchers have considered the simultaneous deployment of both charging methods. In our most recent study (Wang et al., 2022), we analyzed the charging behavior of BEV drivers, comparing their choice between DCFC and charging lanes based on their socio-demographic data and trip information. Chen et al. (2017) attempted to deploy both stationary charging stations and dynamic charging lanes on a single corridor, rather than a transportation network. Liu et al. (2021) developed a bilevel model to optimize the location of charging lanes, aiming to minimize the social cost. They used a stochastic traffic equilibrium model to determine the charging behavior of BEV drivers, with both dynamic charging lanes and stationary charging stations offered as choices. However, in their model, the locations of charging stations were not considered decision variables but were predetermined.

Thus, we aim to bridge the research gap by addressing the following questions: (i) how can we integrate the deployment of both charging stations and charging lanes? and (ii) what is the impact of the traffic equilibrium of BEVs and the power grid operation on each other?

3. Modeling

Suppose there is a joint system that includes both the power grid network and the transportation network. The complexity of the system is therefore very high. Our focus is to make infrastructure deployment decisions, and as such, we make several assumptions to narrow down our analysis:

- The transportation network and the power grid network can be respectively characterized as directed node-link graphs.
- Each node/link on the transportation network is connected to a node (busbar) in the power grid.
- Each node on the transportation network can have a charging station with sufficient charging spots, and each link can be converted into a charging lane.
- All vehicles traveling in the transportation network are identical BEVs.
- The electricity consumption of BEVs depends only on the travel distance. This means we can predetermine the energy consumption on each link.
- The travel time on each link depends on the traffic flow on the link, which captures the congestion effect.

Note that the deployment of charging infrastructures has a significant impact on the charging availability of each node and link, which, in turn, affects the routing choices of BEV drivers. Moreover, the traffic equilibrium achieved by all BEVs affects the charging demand of each node and link and consequently influences the energy distribution of the power grid network. When a large number of BEVs are deployed, the route choices of each driver collectively change the traffic conditions due to congestion. To address these interrelated factors, we propose a bilevel optimization model. The infrastructure deployment decisions and energy distribution decisions serve as the upper-level decision variables, while the route choices of BEV drivers serve as the lower-level decision variables.

At the lower level, each BEV driver is given all the built charging infrastructures and makes the best routing choice considering the travel time and charging cost. We model this routing decision for each driver as a single vehicle problem (SVP) to minimize the corresponding travel cost. The resulting equilibrium from the SVP affects the system-level transportation cost and the power generation cost, which should be carefully evaluated at the upper level to guide the infrastructure deployment decisions.

For reading convenience, we provide a notation table in the Appendix to illustrate all parameters and decision variables.

3.1. Single vehicle problem (SVP)

To begin, we concentrate on the charging decisions associated with a particular BEV driver. Suppose there is a transportation network denoted by $G^0 = (N, A)$, where N is the node set and A is the link set. Charging lanes are deployed on the links, denoted by binary variables $x_a \in \{0,1\}$ for $a \in A$, where $x_a = 1$ indicates link a is a charging lane, and $x_a = 0$ otherwise. Similarly, charging stations are deployed on nodes, denoted by binary variables $y_i \in \{0,1\}$ for $i \in N$. Note that the deployment of charging infrastructures is assumed to be exogenous when we analyze the driver's decision, i.e., x_a and y_i are parameters. We will analyze the deployment decisions later. Further, suppose one BEV driver needs to finish a trip w, with its origin denoted by $o(w) \in N$ and destination denoted by $d(w) \in N$. Among all possible paths connecting $o(w)$ and $d(w)$, denoted by P^w, a particular path $p \in P^w$ is chosen. We let $A(p) \subseteq A$ and $N(p) \subseteq N$ be the respective link and node subsets covered by path p. Then, let d_a be the link length and t_a be the given travel time for passing link $a \in A(p)$. To guarantee the trip can be finished, the driver needs to maintain a certain level of SOC for the BEV by making charging decisions along the path. Let s_a^p be the amount of time the driver chooses to charge the vehicle when driving through a charging lane $a \in A(p)$, where $x_a = 1$, and τ_i^p be the charging time for using a charging station at node $i \in N(p)$, where $y_i = 1$. In addition, we track the SOC of the BEV by L_i^p and l_i^p when it leaves and enters node i, respectively. Two major factors affect the driver's decision: the charging cost and the travel time. Normally, charging through a dynamic charging lane saves time but incurs a higher charging cost, while using the charging station is the opposite. Hence, letting E_l and Γ_l (E_s and Γ_s) be the fixed charging speed and unit charging cost for using charging lanes (charging stations), respectively, the driver incurs a total charging cost as $\sum_{a\in A(p)} s_a^p E_l \Gamma_l + \sum_{i\in N(p)} \tau_i^p E_s \Gamma_s$. As for the travel time, we convert it into the corresponding time cost under a certain time value parameter V. The total time cost, including the charging time on charging stations, can be captured by $V \cdot (\sum_{a\in A(p)} t_a + \sum_{i\in N(p)} \tau_i^p)$. Therefore, the BEV driver seeks the best trade-off by solving the following cost minimization problem,

$$\min_{s_a^p, \tau_i^p, L_i^p, l_j^p} \sum_{a\in A(p)} s_a^p E_l \Gamma_l + \sum_{i\in N(p)} \tau_i^p E_s \Gamma_s + V \cdot \Big(\sum_{a\in A(p)} t_a + \sum_{i\in N(p)} \tau_i^p \Big)$$

s.t.

$$s_a^p \geq 0, \qquad \forall a \in A(p) \tag{1}$$

$$s_a^p \leq t_a^p \cdot x_a, \qquad \forall a \in A(p) \tag{2}$$

$$\tau_i^p \geq 0, \qquad \forall i \in N(p) \tag{3}$$

$$\tau_i^p \leq \frac{E_2}{E_s} \cdot y_i, \qquad \forall i \in N(p) \tag{4}$$

$$E_1 \leq L_i^p, \qquad \forall i \in N(p) \tag{5}$$

$$L_i^p \leq E_2, \qquad \forall i \in N(p) \tag{6}$$

$$L_{o(w)}^p = E_0, \tag{7}$$

$$l_i^p \geq 0 \qquad \forall i \in N(p) \tag{8}$$

$$L_i^p - l_j^p - d_a \Omega + s_a^p E_l = 0, \qquad \forall (i,j) = a \in A(p) \tag{9}$$

$$L_i^p - l_i^p - \tau_i^p E_s = 0, \tag{10}$$

Here, Constraints (2) and (4) guarantee that the driver can only use a charging lane or a charging station if it is deployed at link a or node i, respectively. E_2/E_s is the maximum possible charging time for a BEV at charging stations, charging from 0% to 100% SOC. This is used to bound the charging time decision τ_i^p. Constraints (5) and (6) ensure that the SOC of BEV, when leaving any node, is no less than a safety level E_1 and no larger than the battery capacity E_2. Constraint (7) sets that the BEV leaves the origin with initial SOC E_0. Then, given Ω as the energy consumption rate per unit distance, Constraints (9) and (10) give the energy conservation law for passing through a charging lane and charging station, respectively. To simplify our model, we have assumed that BEV drivers have a uniform initial state of charge (SOC). However, it is possible to extend the model to include multiple classes of BEV drivers with varying initial SOCs. Considering the scope of our work, we have chosen not to expand it with distractive details. Also, note that we consider a general network structure for the transportation network where a road segment can be modeled into multiple consecutive links and virtual nodes. This allows for charging stations to be deployed along the charging lanes, if necessary. The only difference is that deployment decisions for charging lanes may be correlated for these consecutive links, which can be addressed by incorporating grouping constraints as needed.

3.2. Path selection constraints

In the previous section, we provided the charging decision for a single BEV driver based on a chosen path. Now we will extend this to capture the route choice of a large volume of BEVs over the entire network, while considering the congestion effect. Suppose the origin–destination (OD) travel demand is given, denoted by g^w for a particular OD pair $w \in W$. Each BEV driver chooses the path with the minimum travel cost, as mentioned before (which considers both charging and time costs). Note that, with traffic

congestion, the travel time t_a in each link a is no longer a fixed parameter but jointly determined by all BEV drivers passing through, i.e., the traffic volume. Let c_a be the traffic capacity and t_a^0 be the free flow travel time of link a, we will use the widely applied Bureau of Public Roads (BPR) function to estimate the travel time (Dafermos and Sparrow, 1969)

$$t_a = t_a^0 \left[1 + 0.15 \left(\frac{v_a}{c_a} \right)^4 \right], \tag{11}$$

where v_a is the traffic flow. As each driver selects the path with the lowest travel cost among all available paths, all drivers will eventually reach the traffic equilibrium, commonly known as the user equilibrium (UE) proposed by Wardrop and Whitehead (1952). At the UE, no driver can further reduce the travel cost by switching the path. Hence, the travel cost for drivers with the same OD pair w should be equal, denoted by μ^w. Otherwise, a driver can always switch to a different path to reduce the travel cost. Based on this, with SVP across all possible paths, we need to impose additional constraints to guarantee that the traffic reaches the UE. These constraints are as follows:

$$\sum_{p \in P^w} f_p = g^w, \qquad \forall w \in W \tag{12}$$

$$v_a = \sum_{w \in W} \sum_{p \in P^w} f_p \Delta_a^p, \qquad \forall a \in A \tag{13}$$

$$f_p \geq 0, \qquad \forall p \in P^w, \forall w \in W \tag{14}$$

$$\sum_{a \in A(p)} s_a^p E_l \Gamma_l + \sum_{i \in N(p)} \tau_i^p E_s \Gamma_s + V \cdot \Big(\sum_{a \in A(p)} t_a + \sum_{i \in N(p)} \tau_i^p \Big) - \mu^w \geq 0, \qquad \forall p \in P^w, \forall w \in W \tag{15}$$

$$\left(\sum_{a \in A(p)} s_a^p E_l \Gamma_l + \sum_{i \in N(p)} \tau_i^p E_s \Gamma_s + V \cdot \Big(\sum_{a \in A(p)} t_a + \sum_{i \in N(p)} \tau_i^p \Big) - \mu^w \right) \cdot f_p = 0. \qquad \forall p \in P^w, \forall w \in W \tag{16}$$

Here, f_p represents the BEV demand for a specific path p, and $\Delta_a^p \in \{0, 1\}$ is an indicator that shows whether path p covers link a. Constraints (12) shows the flow conservation, ensuring that the total demand over all paths connecting trip w equals the corresponding OD demand. Constraint (13) connects the link flow with the path flow, while Constraint (14) ensures the feasibility of non-negative path flows. Constraints (15) and (16) use a non-linear complementary problem (NCP) to give UE condition. When a path flow is positive, the travel cost of the path is equal to the equilibrium cost μ^w. Conversely, those paths that are not in use ($f_p = 0$) must have a higher cost than μ^w.

3.3. Constraints of power grid

To account for the impact of the charging decisions of a large volume of BEVs on the power grid balance, we now consider the mutual influence between traffic and the power grid. Note that the power network we considered here is the transmission network rather than the local distribution network. Suppose the power grid network is given by $G^1 = (K, H)$, where K is the node set of busbars (Kundur et al., 2004) and H is the link set of transmission lines connecting two busbars. Each busbar k can supply energy to a set of transportation links and nodes, denoted by $\Lambda_{k,l} \subseteq A$ and $\Lambda_{k,s} \subseteq N$, respectively. The lower and upper real power limits of each busbar are given by A_k^l and A_k^u, respectively. Given the traffic equilibrium of the transportation network, the total energy supported by busbar k for charging BEVs can be therefore determined as $\sum_{a \in \Lambda_{k,l}} \sum_{w \in W} \sum_{p \in P^w} f_p \cdot \Delta_a^p \cdot s_a^p \cdot E_l + \sum_{i \in \Lambda_{k,s}} \sum_{w \in W} \sum_{p \in P^w} f_p \cdot \Delta_i^p \cdot \tau_i^p \cdot E_s$. Let Θ_k be the other commercial and residential regular real power load of busbar $k \in K$. To maintain the energy balance on each busbar, power flows occur on transmission lines. For each transmission line $(k, m) \in H$, a thermal limit of real power flow R_{km}, the electrical susceptance D_{km}, and electrical conductance G_{km} are given. Therefore, if we let h_{km} be the power flow in the transmission line from busbar k to busbar m, taking into account the transmission power loss, the energy flow constraints of the power grid can be expressed as follows (Castillo and Gayme, 2017),

$$\begin{aligned} &\phi_k - \Theta_k - \sum_{a \in \Lambda_{k,l}} \sum_{w \in W} \sum_{p \in P^w} f_p \cdot \Delta_a^p \cdot s_a^p \cdot E_l \\ &- \sum_{i \in \Lambda_{k,s}} \sum_{w \in W} \sum_{p \in P^w} f_p \cdot \Delta_i^p \cdot \tau_i^p \cdot E_s - \sum_{(k,m) \in H} h_{km} = 0, \qquad \forall k \in K \end{aligned} \tag{17}$$

$$h_{km}^t = D_{km}(\delta_k - \delta_m), \qquad \forall (k, m) \in H \tag{18}$$

$$h_{km}^l = \frac{1}{2} G_{km} (\delta_k - \delta_m)^2, \qquad \forall (k, m) \in H \tag{19}$$

$$h_{km} = h_{km}^t + h_{km}^l \qquad \forall (k, m) \in H \tag{20}$$

$$-R_{km} \leq h_{km} \leq R_{km}, \qquad \forall (k, m) \in H \tag{21}$$

$$A_k^l \leq \phi_k \leq A_k^u, \qquad \forall k \in K \tag{22}$$

$$\delta_1 = 0. \tag{23}$$

Here, ϕ_k is the real power injection and δ_k is voltage angle (in radians) in busbar k. Constraint (17) gives the power flow balance. Under practical conditions, we can assume the voltage magnitude at each node equals to the base voltage and the angle differences

(i.e., $\delta_k - \delta_m$) between busbars are sufficiently small. Constraints (18) capture the real power transmission due to phase shift over transmission. Constraints (19) characterize the corresponding real power loss due to transmission. The real power branch flow h_{km} considering the power loss is given by Constraint (20). Constraints (21) and (22) ensure the thermal and power injection feasibility. Constraint (23) sets the voltage angle reference node to node 1.

3.4. Upper-level objective function

In the upper level, the system aims to find an optimal plan for deploying charging infrastructure, subject to the lower-level traffic equilibrium and power grid constraints. Recall that the charging infrastructure deployment decisions are captured by binary variables x_a and y_i, where x_a means whether the link a is a charging lane and y_i means whether the node i is a charging station. Here, we consider a total budget Ψ will be allocated with C_l as the building cost of charging lane per unit distance, and C_s as the building cost of a charging station. Under the limited budget, we aim to minimize the total cost of the integrated system, including the total travel cost and the total power generation cost. The Infrastructure Deployment Problem (IDP) can be written as follows,

$$\begin{aligned}
&\min_{\substack{x_i, y_a, \mu^w, \phi_k, f_p, v_a \\ s_a^p, \tau_i^p, L_i^p, l_j^p}} \sum_k Z_k(\phi_k) + \sum_{w\in W} \mu^w \cdot g^w \\
&\text{s.t.} \sum_{a\in A} y_a \cdot d_a \cdot C_l + \sum_{i\in N} x_i \cdot C_s \le \Psi && (24)\\
&\quad x_i, y_a \in \{0,1\}, && \forall i \in N, \forall a \in A \\
&\quad (11)\text{–}(23) \\
&\quad s_a^p, \tau_i^p, L_i^p, l_j^p \in \underset{\text{s.t. } (1)\text{–}(10)}{\arg\min} \left\{ \sum_{a\in A(p)} s_a^p E_l \Gamma_l + \sum_{i\in N(p)} \tau_i^p E_s \Gamma_s + V \cdot \Big(\sum_{a\in A(p)} t_a + \sum_{i\in N(p)} \tau_i^p \Big) \right\}. && (25)
\end{aligned}$$

Here, $Z_k(\phi_k)$ is a polynomial function to estimate the total cost of generating ϕ_k amount of electricity at busbar k, e.g., as follows (He et al., 2013),

$$Z_k(\phi_k) = a_{k,0} \cdot \phi_k^2 + a_{k,1} \cdot \phi_k + a_{k,2}. \tag{26}$$

$\mu^w \cdot g^w$ gives the total transportation cost of OD pair $w \in W$. Constraint (24) limits the total budget of infrastructure deployment.

It is obvious that the IDP is a bilevel nonlinear programming problem, which is extremely difficult to solve in general. In the following section, we will provide a reformulation method to convert it into its tractable counterpart problem.

4. Reformulation

To solve the IDP, we first convert the lower-level SVP into a set of constraints using Karush–Kuhn–Tucker (KKT) conditions. This will convert the bilevel problem into a simpler single level problem. In particular, by defining Lagrangian multipliers $\lambda_{1,a}^p$, $\lambda_{2,a}^p$, $\lambda_{3,i}^p$, $\lambda_{4,i}^p$, $\lambda_{5,i}^p$, $\lambda_{6,i}^p$, $\lambda_{8,i}^p$, $\lambda_{9,ij}^p$, $\lambda_{10,i}^p$ for corresponding constraints (i.e., auxiliary variables $\lambda_{1,a}^p$ tailored for Constraints (1)), we can convert the SVP into the following nonlinear complimentary conditions (where $x \perp y$ indicates $xy = 0$),

$$0 \le s_a^p \perp \lambda_{1,a}^p \ge 0, \qquad \forall a \in A(p), p \in P^w, w \in W \tag{27}$$

$$0 \le \left(t_a \cdot x_a - s_a^p\right) \perp \lambda_{2,a}^p \ge 0, \qquad \forall a \in A(p), p \in P^w, w \in W \tag{28}$$

$$0 \le \tau_i^p \perp \lambda_{3,i}^p \ge 0, \qquad \forall i \in N(p), p \in P^w, w \in W \tag{29}$$

$$0 \le \left(\frac{E_2}{E_s} \cdot y_i - \tau_i^p\right) \perp \lambda_{4,i}^p \ge 0, \qquad \forall i \in N(p), p \in P^w, w \in W \tag{30}$$

$$0 \le (E_1 - L_i^p) \perp \lambda_{5,i}^p \ge 0, \qquad \forall i \in N(p), p \in P^w, w \in W \tag{31}$$

$$0 \le (L_i^p - E_2) \perp \lambda_{6,i}^p \ge 0, \qquad \forall i \in N(p), p \in P^w, w \in W \tag{32}$$

$$0 \le l_i^p \perp \lambda_{8,i}^p \ge 0, \qquad \forall i \in N(p), p \in P^w, w \in W \tag{33}$$

$$E_l \Gamma_l - \lambda_{1,a}^p + E_l \lambda_{9,ij}^p + \lambda_{2,a}^p = 0, \qquad \forall (i,j) = a \in A(p), p \in P^w, w \in W \tag{34}$$

$$E_s \Gamma_s + V - \lambda_{3,i}^p + \lambda_{4,i}^p - E_s \lambda_{10,i}^p = 0, \qquad \forall i \in N(p), p \in P^w, w \in W \tag{35}$$

$$-\lambda_{5,i}^p + \lambda_{6,i}^p + \lambda_{9,ij}^p + \lambda_{10,i}^p = 0, \qquad \forall (i,j) = a \in A(p), p \in P^w, w \in W \tag{36}$$

$$-\lambda_{8,j}^p - \lambda_{9,ij}^p - \lambda_{10,j}^p = 0, \qquad \forall (i,j) = a \in A(p), p \in P^w, w \in W \tag{37}$$

Substituting (25) with these complementary conditions results in a single level problem for the IDP. However, there are still challenges in the nonlinear structure. Apart from the nonlinear complementary conditions, other bilinear terms, and the nonlinear nature of the BPR function also require further problem reduction. One strategy involves breaking the nonlinearity through a series of mixed-integer decisions. By using the linearization method that follows, the IDP can then be transformed into a mixed-integer linear programming problem.

Linearization of non-linear complimentary problem

Consider a representative NCP formulated as $0 \le x \perp y \ge 0$. It is equivalent to the following two linear constraints,

$$0 \le x \le M \cdot \beta,$$
$$0 \le y \le M \cdot (1-\beta),$$

where $\beta \in \{0,1\}$ is a binary variable, and M is a sufficiently large positive number. To establish the upper bound for each variable, we have implemented the big M method. Notably, we have avoided assigning a significantly large positive value to M without careful consideration, but rather opted for a value that reflects the variable's characteristics. In the above equations from (27) to (33), we can use the upper bound of variables in each constraint as the value of M. The subscripts of M reflect the indices of the corresponding constraints.

$$M_{27} = \frac{E_2}{E_l}, \tag{38}$$
$$M_{28} = t_a^0\left[1 + 0.15\left(\frac{\sum_{w\in W}\sum_{p\in P^w} g^w \Delta_a^p}{c_a}\right)^4\right], \forall a \in A(p), p \in P^w, w \in W \tag{39}$$
$$M_{29} = \frac{E_2}{E_s}, \quad \forall a \in A(p), p \in P^w, w \in W \tag{40}$$
$$M_{30} = \frac{E_2}{E_s}, \quad \forall a \in A(p), p \in P^w, w \in W \tag{41}$$
$$M_{31} = E_1, \quad \forall a \in A(p), p \in P^w, w \in W \tag{42}$$
$$M_{32} = E_2, \quad \forall a \in A(p), p \in P^w, w \in W \tag{43}$$
$$M_{33} = E_2, \quad \forall a \in A(p), p \in P^w, w \in W \tag{44}$$

Linearization of bilinear constraints

Consider those bilinear constraints, e.g., $t_a \cdot x_a$ in (1), and $f_p \cdot s_a^p$ and $f_p \cdot \tau_i^p$ in (17). In particular, $t_a \cdot x_a$ is a product of a continuous variable and a binary variable, which can be exactly reformulated with the big M method. Suppose $Q_a = t_a \cdot x_a$, the product can be linearized as follows (Coelho, 2013):

$$Q_a \le M_{Q_a} \cdot x_a, \quad \forall a \in A(p), p \in P^w, w \in W \tag{45}$$
$$Q_a \le t_a, \quad \forall a \in A(p), p \in P^w, w \in W \tag{46}$$
$$Q_a \ge t_a - (1-x_a)\cdot M_{Q_a}, \quad \forall a \in A(p), p \in P^w, w \in W \tag{47}$$
$$Q_a \ge 0, \quad \forall a \in A(p), p \in P^w, w \in W. \tag{48}$$
$$M_{Q_a} = t_a^0\left[1 + 0.15\left(\frac{\sum_{w\in W}\sum_{p\in P^w} g^w \Delta_a^p}{c_a}\right)^4\right], \quad \forall a \in A \tag{49}$$

To choose a proper big M value M_{Q_a}, we allocate the maximum possible traffic on link a and utilize the resulting travel time as the upper bound for Q_a, which is expressed in (49). By adding (45)–(48), the linearization is done by replacing $t_a \cdot x_a$ in (1) and as follows,

$$s_a^p \le Q_a, \quad \forall a \in A(p), p \in P^w, w \in W \tag{2b}$$

Then, $f_p \cdot s_a^p$ and $f_p \cdot \tau_i^p$ are general bilinear terms. We can use a piecewise linear function to represent f_p. The flow of the path f_p could be partitioned into N segments (the estimation error reduces as N increases). In each path, we use a set of values $K_{p,n}$ to partition f_p, and a set of binary variables η_p^n to indicate whether f_p falls in each section, i.e., $K_{p,n} \le f_p < K_{p,n+1}$ if $\eta_p^n = 1$:

$$K_{p,n}\cdot\eta_p^n \le f_p < M_{f_p}\cdot\left(1-\eta_p^n\right) + K_{p,n+1}, \quad \forall p \in P^w, w \in W \tag{50}$$
$$\eta_p^n \in \{0,1\}, \quad \forall p \in P^w, w \in W \tag{51}$$
$$\sum_n \eta_p^n = 1, \quad \forall p \in P^w, w \in W \tag{52}$$
$$M_{f_p} = g^w, \quad \forall p \in P^w, w \in W \tag{53}$$

The upper bound for the variable f_p (the traffic flow of path $p \in P^w$ for OD pair w) is the total traffic demand of OD pair w, which can be used as the big M parameter in the model in (53). Therefore, f_p in (17) could be represented as $\sum_n K_{p,n}\cdot\eta_p^n$. Then the two non-linear terms become two products of one continuous variable and one binary variable. We use the same method above to

linearize two products, i.e. $Q_{1,n}^{p,a} = s_a^p \cdot \eta_p^n$, $Q_{2,n}^{p,i} = \tau_i^p \cdot \eta_p^n$, then constraint (17) can be linearized as follows:

$$\phi_k - \Theta_k - \sum_{a\in\Lambda_{k,l}} \sum_{w\in W} \sum_{p\in P^w} \sum_n K_{p,n} \cdot \Delta_a^p \cdot E_l \cdot Q_{1,n}^{p,a} - \sum_{i\in\Lambda_{k,l}} \sum_{w\in W} \sum_{p\in P^w} \sum_n K_{p,n} \cdot \Delta_i^p \cdot E_s \cdot Q_{2,n}^{p,i} - \sum_{(k,m)\in H} h_{km} = 0, \qquad \forall k \in K \tag{54}$$

And we should add constraint (50)–(52) as well as the constraints of the products by one continuous variable and one binary variable:

$$Q_{1,n}^{p,a} \le M_{Q_1} \cdot \eta_p^n, \qquad \forall a \in A(p), p \in P^w, w \in W \tag{55}$$

$$Q_{1,n}^{p,a} \le s_a^p, \qquad \forall a \in A(p), p \in P^w, w \in W \tag{56}$$

$$Q_{1,n}^{p,a} \ge s_a^p - (1-\eta_p^n) \cdot M_{Q_1}, \qquad \forall a \in A(p), p \in P^w, w \in W \tag{57}$$

$$Q_{1,n}^{p,a} \ge 0, \qquad \forall a \in A(p), p \in P^w, w \in W \tag{58}$$

$$M_{Q_1} = \frac{E_2}{E_l}, \qquad \forall a \in A(p), p \in P^w, w \in W \tag{59}$$

$$Q_{2,n}^{p,i} \le M_{Q_2} \cdot \eta_p^n, \qquad \forall i \in N(p), p \in P^w, w \in W \tag{60}$$

$$Q_{2,n}^{p,i} \le \tau_i^p, \qquad \forall i \in N(p), p \in P^w, w \in W \tag{61}$$

$$Q_{2,n}^{p,i} \ge \tau_i^p - (1-\eta_p^n) \cdot M_{Q_2}, \qquad \forall i \in N(p), p \in P^w, w \in W \tag{62}$$

$$Q_{2,n}^{p,a} \ge 0, \forall a \in A(p), \qquad \forall i \in N(p), p \in P^w, w \in W \tag{63}$$

$$M_{Q_2} = \frac{E_2}{E_s}, \qquad \forall i \in N(p), p \in P^w, w \in W \tag{64}$$

The upper bound for the variable $Q_{1,n}^{p,a}$ is determined by charging time of BEV in charging link a of path p, denoted as s_a^p. Specifically, we allocate charging time for BEV from 0% to 100% SOC (E_2) as the big M parameter in the model in (59). Similarly, the upper bound for the variable $Q_{2,n}^{p,i}$ is determined by charging time of BEV in charging node i of path p, denoted as τ_i^p. We allocate charging time for BEV from 0% to 100% SOC as well of the big M parameter in (64).

Linearization of other nonlinear constraints

Our problem includes three constraints that involve nonlinear functions: the travel time function (11), the electricity generation cost function (26), and the power loss function (19). To address this issue, we can use a piecewise linear function to represent the two functions by partitioning the flow on the link v_a, partitioning the injection flow on each busbar ϕ_k into N segments, and partitioning voltage angle difference $(\delta_k - \delta_m)$, respectively, similar to the linearization process of flow f_p on each path.

In each link, we use a set of values $K_{a,n}$ to partition v_a and a set of binary variables $\xi_{a,n}$ to indicate whether v_a falls in the section $[K_{a,n}, K_{a,n+1})$, i.e., $K_{a,n} \le v_a < K_{a,n+1}$ if $\xi_a^n = 1$. In each segment, we build an approximately linear function to represent the travel time t_a:

$$t_a = A_n^a \cdot v_a + B_n^a \tag{65}$$

where A_n^a and B_n^a are two coefficients to be determined. We use the first-order Taylor series to determine them as follows:

$$A_n^a = \left.\frac{dt_a}{dv_a}\right|_{K_{a,n}} = 0.6 * \frac{t_a^0}{c_a^4} * K_{a,n}^3 \tag{66}$$

$$B_n^a = t_a^0[1 + 0.15(\frac{K_{a,n}}{c_a})^4] \tag{67}$$

Therefore, rewrite the travel time function into mixed-integer linear constraints:

$$K_{a,n} \cdot \xi_{a,n} \le v_a < M_{v_a} \cdot (1-\xi_{a,n}) + K_{a,n+1}, \qquad \forall a \in A(p), p \in P^w, w \in W, n \in N \tag{68}$$

$$(-M_{t_n^a}) \cdot (1-\xi_{a,n}) \le t_a - (A_n^a \cdot v_a + B_n^a) \le M_{t_n^a} \cdot (1-\xi_{a,n}), \qquad \forall a \in A(p), p \in P^w, w \in W, n \in N \tag{69}$$

$$\xi_{a,n} \in \{0,1\}, \qquad \forall a \in A(p), p \in P^w, w \in W, n \in N \tag{70}$$

$$\sum_n \xi_{a,n} = 1, \qquad \forall i \in N(p), p \in P^w, w \in W, n \in N \tag{71}$$

$$M_{v_a} = \sum_{w\in W} \sum_{p\in P^w} g^w \Delta_a^p \qquad \forall a \in A(p), p \in P^w, w \in W \tag{72}$$

$$M_{t_n^a} = \sum_{w\in W} \sum_{p\in P^w} g^w \Delta_a^p - B_n^a \qquad \forall i \in N(p), p \in P^w, w \in W, n \in N \tag{73}$$

where M_{v_a} is the upper bound of volume in link a, computed in (72), and $M_{t_n^a}$ is the upper bound of $t_a - (A_n^a \cdot v_a + B_n^a)$, computed in (73). The upper bound of $t_a - (A_n^a \cdot v_a + B_n^a)$ is derived when t_a is maximum and $v_a = 0$. Binary variable $\xi_{a,n}$ indicates that whether v_a is no less than $K_{a.n}$. From (68), if $\xi_{a,n} = 0$, then $0 \le v_a < M_{v_a}$; if $\xi_{a,n} = 1$, then $K_{a,n} \le v_a < K_{a,n+1}$. And in constraints (69), we have if $\xi_{a,n} = 1$ (which indicates v_a falls into $[K_{a,n}, K_{a,n+1})$), then $0 \le t_a - (A_n^a v_a + B_n^a) \le 0$, i.e., $t_a = (A_n^a v_a + B_n^a)$.

Similarly, we could linearize the electricity generation cost function (26) as follows:

$$C_n^k = \left.\frac{dZ_k}{d\phi_k}\right|_{K_{k,n}} = 2a_{k,0} \cdot K_{k,n} + a_{k,1}, \qquad \forall k \in K, n \in N \tag{74}$$

$$D_n^k = a_{k,0} \cdot K_{k,n}^2 + a_{k,1} \cdot K_{k,n} + a_{k,2} - C_n^k \cdot K_{k,n}, \qquad \forall k \in K, n \in N \tag{75}$$

$$K_{k,n} \cdot \theta_{k,n} \le \phi_k < M_{\phi_k} \cdot (1 - \theta_{k,n}) + K_{k,n+1} \qquad \forall k \in K, n \in N \tag{76}$$

$$(-M_{Z_k}) \cdot (1 - \theta_{k,n}) \le Z_k - (C_n^k \cdot \phi_k + D_n^k) \le M_{Z_k} \cdot (1 - \theta_{k,n}), \qquad \forall k \in K, n \in N \tag{77}$$

$$\theta_{k,n} \in \{0, 1\}, \qquad \forall k \in K, n \in N \tag{78}$$

$$\sum_n \theta_{k,n} = 1, \qquad \forall k \in K, n \in N \tag{79}$$

$$M_{\phi_k} = A_k^u \qquad \forall k \in K \tag{80}$$

$$M_{Z_k} = a_{k,0} \cdot A_k^u + a_{k,1} \cdot A_k^u + a_{k,2} - D_n^k \qquad \forall k \in K, n \in N \tag{81}$$

We can also linearize the power loss function 19 as follows (we treat $(\delta_k - \delta_m)$ as a variable and partitioning the difference):

$$E_n^{km} = \left.\frac{dh_{km}^l}{d(\delta_k - \delta_m)}\right|_{K_{km,n}} = G_{km}(\delta_k - \delta_m), \qquad \forall (k,m) \in H, n \in N \tag{82}$$

$$F_n^{km} = \frac{1}{2} G_{km} (K_{km,n})^2 - E_n^{km} \cdot K_{km,n}, \tag{83}$$

$$K_{km,n} \cdot \kappa_{km,n} \le \delta_k - \delta_m < M_{\delta_{km}} \cdot (1 - \kappa_{k,n}) + K_{km,n+1} \qquad \forall (k,m) \in H, n \in N \tag{84}$$

$$(-M_{h_{km}^n}) \cdot (1 - \kappa_{km,n}) \le h_{km}^l - (E_n^{km} \cdot (\delta_k - \delta_m) + F_n^{km}) \le M_{h_{km}^n} \cdot (1 - \kappa_{km,n}), \forall (k,m) \in H, n \in N \tag{85}$$

$$\kappa_{km,n} \in \{0, 1\}, \qquad \forall (k,m) \in H, n \in N \tag{86}$$

$$\sum_n \kappa_{km,n} = 1, \qquad \forall (k,m) \in H, n \in N \tag{87}$$

$$M_{\delta_{km}} = 4\pi \qquad \forall (k,m) \in H \tag{88}$$

$$M_{h_{km}^n} = \frac{1}{2} G_{km} \cdot (4\pi)^2 - (E_n^{km} \cdot (-4\pi) + F_n^{km}) \qquad \forall (k,m) \in H, n \in N \tag{89}$$

Since δ_k and δ_m are in radians and can be negative, the maximum difference $(\delta_k - \delta_m)$ is $2\pi - (-2\pi) = 4\pi$ in (88). The upper bound of $h_{km}^l - (E_n^{km} \cdot (\delta_k - \delta_m) + F_n^{km})$ is computed in (89).

After implementing all the reformulations described above, we have successfully converted the IDP into a mixed-integer linear optimization problem, which can be easily solved using commercial solvers such as Gurobi.

5. Numerical analysis

This section provides a numerical example to demonstrate the effectiveness of our model and the solution algorithm. Additionally, we perform a sensitivity analysis by systematically varying the traffic demand, the electricity generation of each busbar, and the infrastructure cost of charging lanes to assess their corresponding effects on our results.

5.1. The integrated transportation and power grid network

We consider a nine-node road network and a subset of the IEEE 118-busbar system as shown in Fig. 1. This is a typical medium-sized traffic network (He et al., 2013), and includes 32 links and 32 OD pairs. The free-flow travel speed is set at 60 miles/h, and Table 1 provides the length, free-flow travel time, and capacity of each link. The traffic demand for each OD pair is given in Table 2. For the power grid, we build twelve busbars numbering from 10 to 21, with each busbar serving a road (two directions) or a node or both on the transportation network. The transmission lines are undirected and connect busbars in the power network. Table 3 provides the input data for each generator, and Table 4 shows the attributes of each transmission line.

Then we decide the parameters in our numerical analysis. We use the average income in the U.S. in 2019, $26.5 per hour per capita, as the value of travel time V (Dey and Loewenstein, 2020). The battery capacity, E_2, is 40 kWh, a type of Nissan Leaf BEV (Iora and Tribioli, 2019). The energy consumption rate, Ω, is 0.29 kWh/mi. The charging lane's charging speed E_l is 6 kW (Manshadi et al., 2017), and the charging power of DCFC charging E_s we use is 100 kW, which is one of the versions of the Tesla Supercharger (Chen and Perez, 2018). The charging price of charging lanes Γ_l is $0.5 per kWh (Manshadi et al., 2017), and

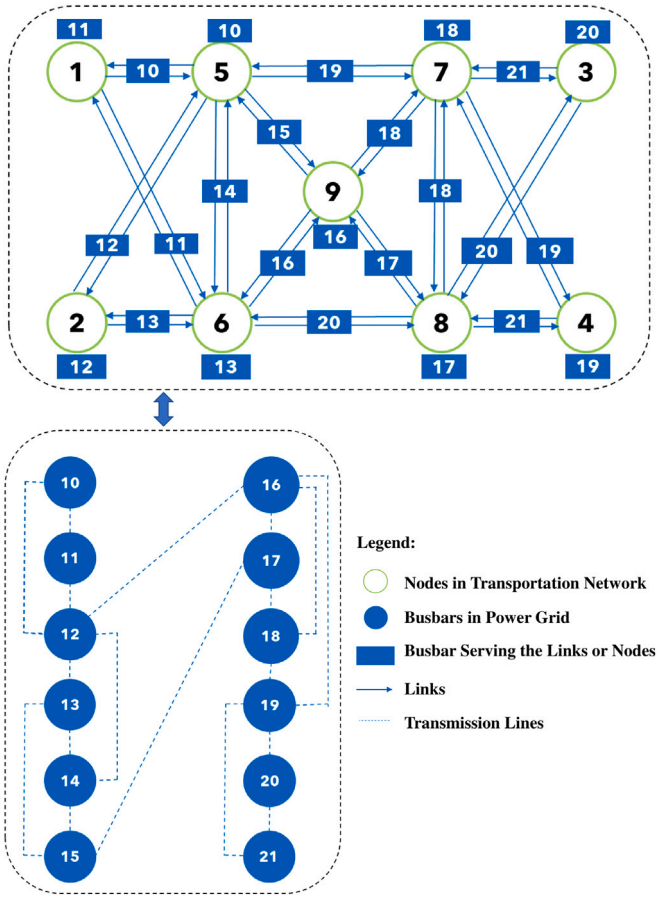

Fig. 1. Numerical analysis road network.

Table 1
Link length (Mile), free-flow travel time (min), and capacity (10^3 veh/h).

Link	Length	Free-flow travel time	Capacity	Link	Length	Free-flow travel time	Capacity
1-5	62	62	15	5-1	62	62	15
1-6	102	102	24	6-1	102	102	24
2-5	104	104	26	5-2	104	104	26
2-6	64	64	17	6-2	64	64	17
3-7	59	59	14	7-3	59	59	14
3-8	99	99	23	8-3	99	99	23
4-7	101	101	26	7-4	101	101	26
4-8	64	64	18	8-4	64	64	18
5-6	81	81	29	6-5	81	81	29
5-7	79	79	31	7-5	79	79	31
5-9	56	56	36	9-5	56	56	36
6-8	78	78	29	8-6	78	78	29
6-9	55	55	39	9-6	55	55	39
7-8	84	84	31	8-7	84	84	31
7-9	55	55	36	9-7	55	55	36
8-9	57	57	37	9-8	57	57	37

that of the charging station Γ_s is \$0.3 per kWh (Muratori et al., 2019). We set the initial SOC E_0 of all BEV to be 20 kWh, i.e., 50% of the capacity, for demonstration convenience. Besides, we set the minimum SOC drivers trying to maintain E_1 as 2 kWh.

To estimate the infrastructure cost, we used the parameters provided by Suomalainen and Colet (2019). In their paper, they provided two types of charging facilities, charging lanes and DCFC charging stations, to supply electricity to BEVs over a 200 km (124 miles) highway. They computed the infrastructure costs of the two charging methods, including the initial installation, material, maintenance, and replacement costs for 25 years (from 2020 to 2045). To ensure all vehicles could finish their trip, they built a charging station every 30 km, and the charging lane length is also 30 km. The total costs of charging stations over 25 years are

Table 2
Travel demand for each O-D.

OD	Traffic demand	OD	Traffic demand	OD	Traffic demand	OD	Traffic demand
1-2	500	2-6	520	4-7	600	6-8	500
2-1	550	6-2	500	7-4	650	8-6	480
1-5	600	3-4	500	4-8	550	6-9	512
5-1	650	4-3	550	8-4	530	9-6	520
1-6	700	3-7	600	5-7	590	7-9	420
6-1	750	7-3	650	7-5	600	9-7	470
2-5	535	3-8	700	5-9	630	8-9	490
5-2	530	8-3	750	9-5	625	9-8	481

Table 3
Input data for generators.

BusBar	Regular load (MW)	Lower limit (MW)	Upper limit (MW)	$a_{k,0}$ ($/MW^{2}h)	$a_{k,1}$ ($/MWh)	$a_{k,2}$ ($/h)
10	63	25	110	0.0128	17.82	10.15
11	84	25	110	0.0128	17.82	10.15
12	150	50	210	0.0139	13.29	39
13	78	0	0	0	0	0
14	0	50	210	0.0139	13.29	39
15	77	25	110	0.0128	17.82	10.15
16	0	0	0	0	0	0
17	0	0	0	0	0	0
18	39	100	420	0.0136	8.34	64.16
19	28	0	0	0	0	0
20	0	0	0	0	0	0
21	0	80	300	0.0109	12.89	6.78

Table 4
Input data for transmission lines.

Line	Capacity	Susceptance (D)	Conductance (G)	Line	Capacity	Susceptance (D)	Conductance (G)
10-11	175	66.23	19.12	16-17	500	50	4.22
11-12	175	3.98	1.18	15-17	500	37.31	0
10-12	175	4.63	0.97	16-18	175	4.59	0.97
12-13	175	6.90	1.44	16-19	175	8.55	1.80
12-14	175	6.67	1.39	18-19	175	9.85	2.07
13-14	500	74.07	13.76	19-20	175	3.6	1.00
13-15	175	17.83	3.73	19-21	500	27.03	0
14-15	175	26.60	5.54	20-21	500	62.5	5.04
12-16	500	25.91	0				

$127.12M ($19.07M per station), and the total costs of charging lanes are $202.18M ($1.63M per mile). We used the infrastructure data from their paper and set the budget limit to be $3.85B.

5.2. Model results

We solve the problem under the parameter settings in Section 5.1 using Gurobi. The results of the transportation network are shown in Table 5. According to Table 5, some of the links have zero volume, which indicates that some of the drivers only use the path with charging lanes. Besides, since the roads' capacities are much higher than the traffic volume, the travel time is close to the free-flow travel time on each link. Fig. 2 shows construction plans for charging facilities.

In Fig. 2, the green nodes mean the nodes constructed as charging stations, and the green links indicate that the links are built as charging lanes. The shade of the color represents the volumes on each link: the dark color represents high volume. It can be noted from Fig. 2 that charging facilities' locations have a high relationship with traffic distribution. Under our traffic conditions, more BEV drivers tend to choose charging lanes. For example, most of the traffic from OD 2-1 uses path 2-6-5-1, while only a minimal volume uses path 2-6-1. This can be attributed that path 2-6-5-1 has a charging lane on the link 6-5, on the contrary path 2-6-1 only has a charging station at node 6. The drivers insist on choosing the charging lanes on path 2-6-5-1 even though the travel distance is longer than path 2-6-1.

For the power generation and busbar costs, the details are given in Table 6. It is observed that busbar 18 generates the most electricity to minimize the total cost. The objective value (i.e., the total electricity generation cost plus the total transportation cost) is $763,995.84 ($9234.52 electricity generation cost plus $754,761.32 transportation cost). The total real power loss is 2.73 MW, and the real power generated is 646.71 MW. It can be inferred that the transportation cost is much higher than the electricity generation cost in our model.

Among all the 18,233 BEV traffic on our network, 12,722 of them (69.8%) used the charging lanes, while only 9415 of them (51%) used the charging stations. The average charging time for the vehicles using charging lanes is 41.82 min, whereas the average

Table 5
Equilibrium link conditions.

Link	Volume (veh/h)	Travel time (min)	Link	Volume (veh/h)	Travel time (min)
1-5	850	62	5-1	1950	62
1-6	950	102	6-1	0	0
2-5	0	0	5-2	780	104
2-6	1605	64	6-2	750	64
3-7	1100	59	7-3	900	59
3-8	700	99	8-3	1050	99
4-7	850	101	7-4	1150	101
4-8	850	64	8-4	0	0
5-6	0	0	6-5	2972	81
5-7	590	79	7-5	600	79
5-9	1142	56	9-5	0	0
6-8	500	78	8-6	480	78
6-9	0	0	9-6	1145	55
7-8	0	0	8-7	0	0
7-9	420	55	9-7	470	55
8-9	490	57	9-8	481	57

Table 6
Power generation and cost at each busbar.

Busbar	Electricity generated (MW)	Generation cost ($)	Busbar	Electricity generated (MW)	Generation cost ($)
10	35.17	652.68	16	0	0
11	35.17	652.68	17	0	0
12	70.28	1041.63	18	290.20	3629.68
13	0	0	19	0	0
14	70.28	1041.63	20	0	0
15	35.17	652.68	21	110.46	1563.55

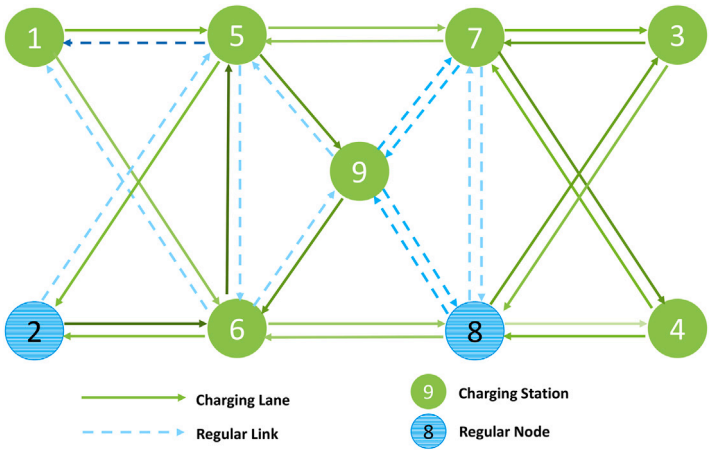

Fig. 2. Deployment solution of charging facilities. (For interpretation of the references to color in this figure legend, the reader is referred to the web version of this article.)

charging time for the vehicles using charging stations is only about 10.34 min. Our results indicate that most BEV drivers prefer to use charging lanes, and the corresponding charging time using charging lanes is much longer than charging stations. Even with higher costs, they like to charge the vehicle while driving instead of waiting at charging stations.

5.3. Sensitivity analysis

In addition to the numerical results, we varied the demand for battery electric vehicles (BEVs) in each origin–destination pair, the upper bound of electricity generation for each busbar, and the infrastructure costs of charging lanes to observe their effects. The sensitivity analysis is presented in three subfigures (Figs. 3a, 3b, and 3c) below, which show the results of varying traffic demand. In these figures, the x-axis represents the traffic demand ratio to the default values in Table 2 for each origin–destination pair. Fig. 3a shows that when traffic demand increases, both the total costs and transportation costs increase, and when the traffic demand is high, the increasing rates of the two costs are higher. Fig. 3b shows that the use of charging lanes and charging stations increases with higher traffic demand. When the demand is twice the original, the volume of charging stations volume exceeds that of charging

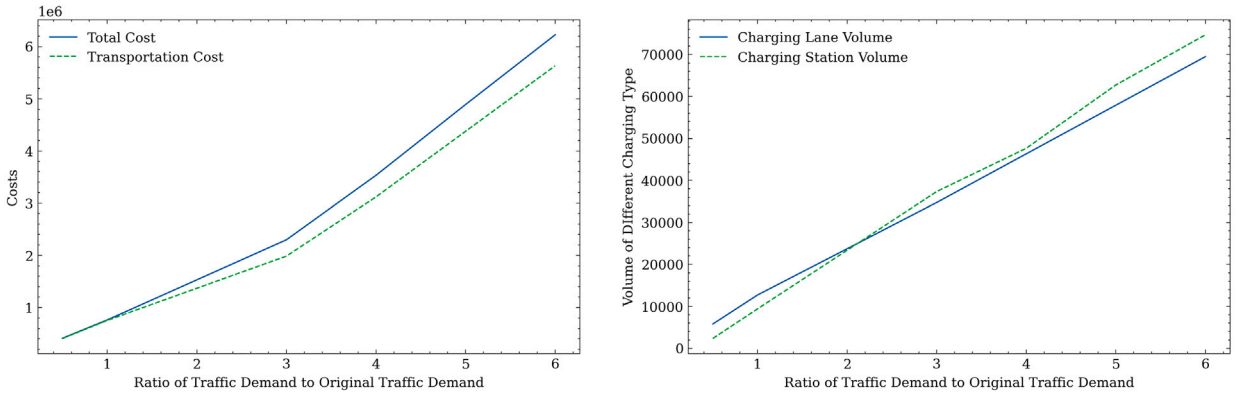

Fig. 3a & b. Costs and volume vs. ratio of traffic demand to original traffic demand.

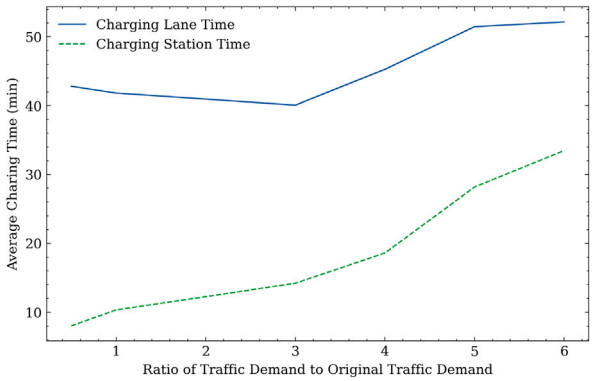

Fig. 3c. Average charging time vs. traffic demand ratio to original.

lanes. Fig. 3c shows that as the demand increases, the average charging time at both charging facilities increases. This indicates that some drivers who initially use the charging lane but have a low charging time would prefer to use the charging station. We think this is because of the electricity generation limit of busbars that supply the charging lanes. This implies that the charging lane serves as the backbone, while the charging station serves as flexible backup resources. Therefore, we will further adjust the upper bound of electricity generation for busbars to examine how the values change.

Further, the sensitivity analysis results of the Electricity Generation Upper Bound of Busbars in the electricity network are presented in three subfigures (Figs. 4a, 4b, and 4c). The x-axis in these figures represents the electricity generation upper bound ratio to the default values in Fig. 3 for busbars. To examine the impact of higher demand, we used the highest demand level in Fig. 3 (six times the original demand). Figs. 4a reveals that increasing the capacity of busbars to supply more electricity results in decreased total costs and transportation costs, provided that we ignore the costs of increasing the capacity of busbars. Fig. 4b shows that as the electricity generation upper bound increases, more BEVs choose to use charging lanes. And Fig. 4c indicates that the average charging time decreases when busbars can generate more electricity. Although the average charging time decreases slightly, considering that more vehicles opt to use charging lanes, the decrease in the total charging time is significant. This suggests that the power grid capacity is a critical factor for supporting BEVs with charging lanes and that charging lanes are more cost-effective than charging stations. Since the demand remains constant and more vehicles use charging lanes, the total cost and transportation cost decrease.

We also investigated the increase in investment in charging infrastructure relative to the distance traveled by BEVs. In this scenario, we calculated the total increase in BEV distances using the charging lane from the lowest busbar capacity to the highest. The result showed an increase of 166,533 miles (equivalent to 1.22 miles per vehicle), while the total increase in the constructed charging lane was 114 miles. We used an infrastructure cost of $1.63M per mile for charging lanes. Under high transportation demand conditions, the converting ratio of the charging lane was found to be 896.2 miles per million dollars. This ratio is highly dependent on the volume of charging lane usage.

The above four subfigures (Figs. 5a, 5b, 5c, and 5d) show the sensitivity analysis of charging lane infrastructure cost. The vertical red line represents the original charging lane infrastructure cost ($1.63M per mile). Fig. 5a shows that when the infrastructure cost decreases, the total cost and the transportation cost also decrease. Fig. 5b shows that with a lower charging lane infrastructure cost, the volume of charging lane usage increases, while the volume of charging station usage decreases. Additionally, the average

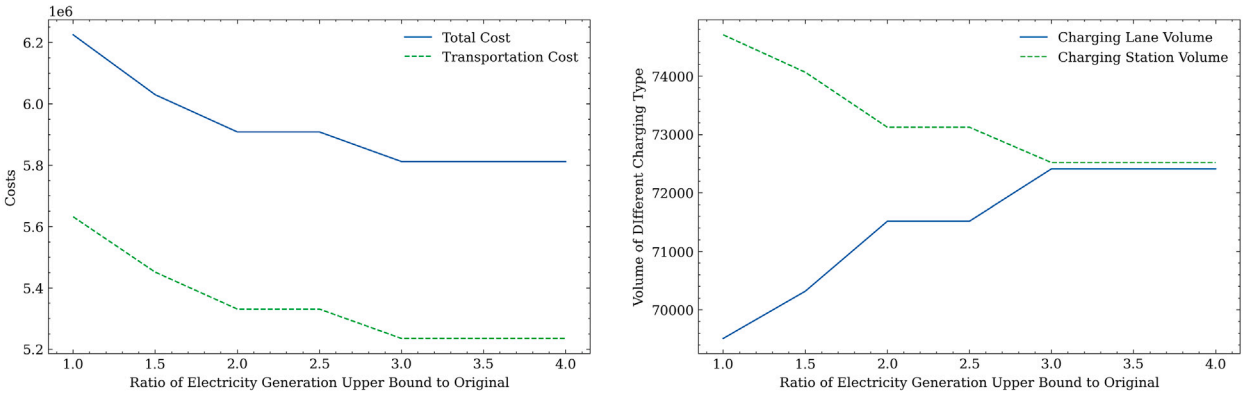

Fig. 4a & b. Costs and volume vs. ratio of electricity generation upper bound to original.

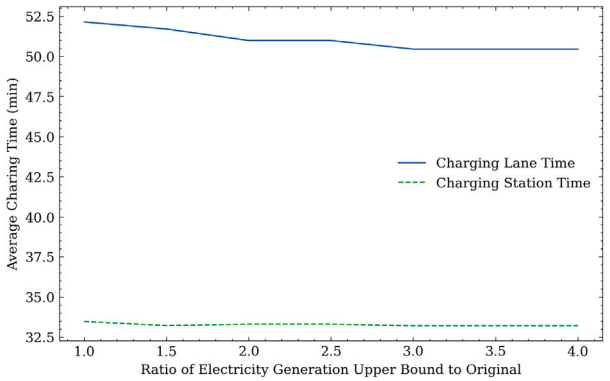

Fig. 4c. Average charging time vs. ratio of electricity generation upper bound to original.

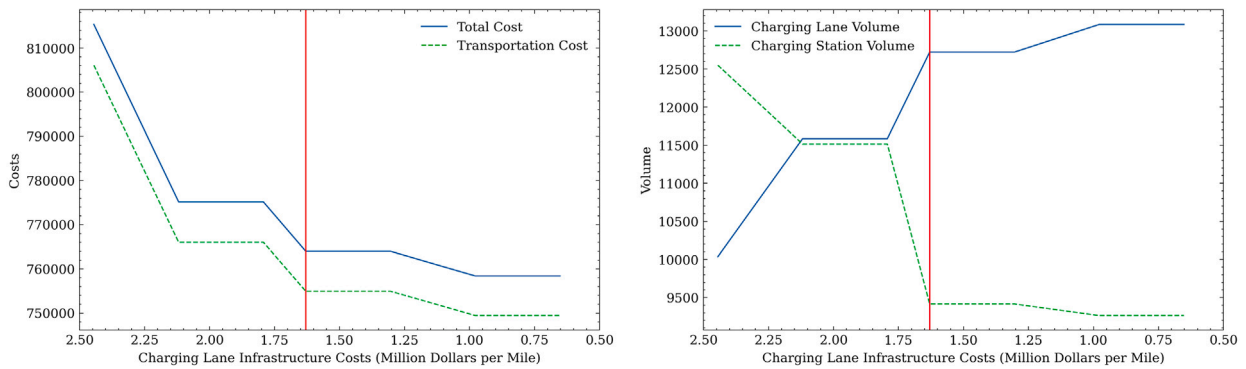

Fig. 5a & b. Costs and volume vs. charging lane infrastructure cost.

charging time for both charging methods decreases as illustrated in Fig. 5c. Fig. 5d shows that when the cost decreases, more charging lanes are built while fewer charging stations are constructed. These results indicate that on the one hand, when the charging lane's infrastructure cost decreases, more charging lanes and fewer charging stations should be constructed, and the total cost decreases. This tells us that the current charging lane cost is satisfying. Lower charging lane cost will not change the number of charging lanes and demand volume. On the other hand, with an increase in infrastructure cost, more BEV drivers tend to use charging stations, and the construction of charging lane miles decreases significantly. The total construction cost of charging lanes remains similar, but the system's total cost increases significantly. Therefore, the efficiency of investment in charging lanes is drastically reduced when the charging lane cost increases.

Finally, we investigate the effects of traffic demand changes on the electricity generation of each busbar. As shown in the Fig. 6, the results indicate that an increase in traffic demand affects the electricity generation of each busbar asynchronously. Specifically,

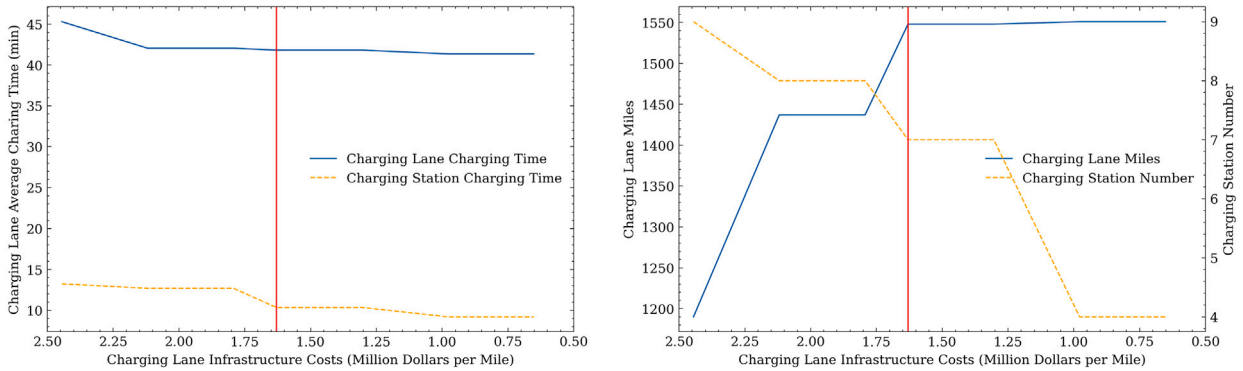

Fig. 5c & d. Average charging time and charging facility construction vs. charging lane infrastructure cost.

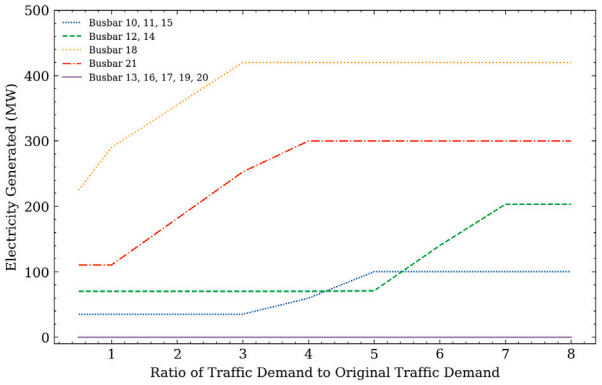

Fig. 6. Electricity generated of each busbar as traffic demand increases.

busbar 18 reacts the first until it reaches its upper real power limits, followed by busbar 21, and then busbars 10, 11, and 15. Busbars 12 and 14 react the last, while the remaining busbars are set to not provide electricity. It is worth noting that the per-unit generation cost determines the sequence of ramping up, where busbars with lower unit costs are ramped up first.

6. Conclusion and discussion

This paper designs a bi-level optimization model to determine the optimal locations of charging facilities and the generator strategy for a given road network and a power grid, while considering traffic assignment and power grid constraints. The lower level of the model focuses on the single vehicle problem: given locations of charging lanes and charging stations, how each driver chooses their path, the charging method, and the charging time at each charging facility from the origin to the destination. The upper level seeks to find the optimal locations of charging facilities and the electricity generated in each busbar in the power grid. To solve the bi-level optimization model, the KKT condition is applied to transform it into a single-level nonlinear optimization problem, which is then linearized using auxiliary binary variables and solved using commercial solvers.

Based on our model, the infrastructure deployment decision maker can decide where to build the charging lanes and fast-charging stations and the corresponding electricity generated in each busbar in the power grid. All BEV drivers can choose their optimal travel paths based on their origin and destination, considering the travel time and the charging cost, to form a traffic equilibrium. Then, the proposed optimization framework is validated via systematic numerical studies. The numerical results show that charging lanes are more cost-effective and attractive than charging stations under reasonable infrastructure cost estimations. Moreover, the total charging time using charging lanes is higher than that of charging stations, and the charging lane serves as the backbone charging resource while charging stations provide flexible complementary charging options. The power grid capacity is a crucial factor in supporting BEVs with charging lanes. Our sensitivity analysis indicates that a reduction in the infrastructure cost of charging lanes can significantly increase the efficiency of investment and attract more BEV drivers to use them. Finally, the results suggest that there is a turning point at which charging lanes can gradually replace charging stations.

The proposed work also has some limitations. First, due to the nonlinear model structure, we can only solve small to moderate-scale problems with commercial solvers. To handle the city-scale transportation network, dimension reduction techniques will be necessary to implement our framework. For example, certain network nodes and links can be grouped together. More advanced optimization framework designed to handle the lower-level traffic equilibrium on a large scale is also needed to be explored. Second,

our work only considers a centralized integration system of systems, i.e., the power grid and the charging infrastructure planner are coordinated to achieve the best social optimum. However, in reality, multiple stake holders with different or even conflicted objectives are in place. The mechanism to achieve the coordination need to be further investigated, e.g., utilizing pricing instrument to create a win–win solution. Some recent studies have been conducted along this direction (Alizadeh et al., 2016; Ding et al., 2022; Qin et al., 2020; Ding and Jian, 2022). We will utilize these work as building block to create benevolent coordination scheme for multiple stake holders.

CRediT authorship contribution statement

Xiasen Wang: Conceptualization, Methodology, Software, Validation, Writing – original draft. **Jiwan Jiang:** Software, Data curation, Investigation, Visualization, Writing – original draft, Writing – review & editing. **Yang Zhou:** Visualization, Investigation, Writing – review & editing. **Xin Wang:** Supervision, Methodology, Writing – review & editing.

Declaration of competing interest

The authors declare that they have no known competing financial interests or personal relationships that could have appeared to influence the work reported in this paper.

Data availability

The authors are unable or have chosen not to specify which data has been used.

Acknowledgment

This research is supported in part by the U.S. National Science Foundation through Grants CNS# 1637772.

Appendix. Notation table

Notations of Transportation Network

Parameters	Description
$G^0(N, A)$	The transportation network. N denotes the set of nodes, A denotes the set of links.
a	$a = (i, j) \in A$, represents a link connecting nodes from i to j.
W	Set of O-D pairs, w means one O-D pair, $w \in W$
P^w	Set of paths between O-D pair w, $p \in P^w$ represents one path belonging to a path set.
$A(p)$	Set of links belonging to path p
$N(p)$	set of nodes belonging to path p.
Δ_a^p	Path-link incidence, where the value equals to 1 if path p passes link a and 0 otherwise.
Δ_i^p	Path-node incidence, where the value equals to 1 if path p passes node i and 0 otherwise.
g^w	demand of O-D pair w
$o(w), d(w)$	Origin and destination of O-D pair w
d_a	Distance of link a
E_0	Initial SOC of BEVs
E_1	Minimum SOC drivers need to maintain
E_2	Maximum battery capacity
Ω	Electricity consumption rate of BEVs per unit distance
E_l	Charging speed of charging lane per unit time
E_s	Charging speed of charging station per unit time
Γ_l	Electricity cost of charging lane
Γ_s	Electricity cost of charging station
V	Value of travel time for BEV drivers
C_l	Cost for one mile of charging lane construction
C_s	Cost for one charging station construction
Ψ	Total budget to build all charging facilities
t_a^0	The free flow travel time of link a
c_a	The traffic capacity of link a
Decision variables	**Description**
t_a	Travel time of BEVs on link a
f_p	Traffic flow on path p
v_a	Traffic flow on link a

s_a^p	Charging time of BEVs on charging link a of path p
τ_i^p	Charging time of BEVs on charging station $i \in N$ along path p
L_i^p	SOC of BEV when leaving the node $i \in N$ along path p
l_i^p	SOC of BEV when entering the node $i \in N$ along path p
x_a	Whether to build a charging lane on link a, binary variable
y_i	Whether to build a charging station on node i, binary variable
μ^w	The travel cost for drivers with the same OD pair w

Notations of Power Grid

Parameters	Description
$G^1(H, K)$	The power grid, where K denotes the set of busbars in the power grid. H is the set of transmission lines in the system
A_k^l, A_k^u	The lower and upper real power limit on a busbar k
Θ_k	The given regular real power load in a busbar k excluding the BEV charging
R_{km}	Thermal limit of real power flow in the transmission line from busbar k to busbar m
D_{km}	The suseptance of a transmission line
G_{km}	The conductance of a transmission line
$\Lambda_{k,l}$	Set of links powered by the busbar k
$\Lambda_{k,s}$	Set of nodes powered by the busbar k
Decision variables	**Description**
ϕ_k	Real power in a busbar k
δ_k	Base apparent power and voltage angle (in radians) in busbar k
h_{km}	Power flow in transmission line from busbar k to busbar m
h_{km}^t	Real power transmission flow without considering the power loss from busbar k to m
h_{km}^l	Real power loss for the power transmission flow from busbar k to m

References

Adenaw, L., Krapf, S., 2022. Placing BEV charging infrastructure: Influencing factors, metrics, and their influence on observed charger utilization. World Electr. Veh. J. 13 (4), 56.

Alizadeh, M., Wai, H.-T., Chowdhury, M., Goldsmith, A., Scaglione, A., Javidi, T., 2016. Optimal pricing to manage electric vehicles in coupled power and transportation networks. IEEE Trans. Control Netw. Syst. 4 (4), 863–875.

Berman, O., Larson, R.C., Fouska, N., 1992. Optimal location of discretionary service facilities. Transp. Sci. 26 (3), 201–211.

Bonges III, H.A., Lusk, A.C., 2016. Addressing electric vehicle (EV) sales and range anxiety through parking layout, policy and regulation. Transp. Res. A 83, 63–73.

Castillo, A., Gayme, D.F., 2017. Evaluating the effects of real power losses in optimal power flow-based storage integration. IEEE Trans. Control Netw. Syst. 5 (3), 1132–1145.

Chen, Z., He, F., Yin, Y., 2016. Optimal deployment of charging lanes for electric vehicles in transportation networks. Transp. Res. B 91, 344–365.

Chen, Z., Liu, W., Yin, Y., 2017. Deployment of stationary and dynamic charging infrastructure for electric vehicles along traffic corridors. Transp. Res. C 77, 185–206.

Chen, Y., Perez, Y., 2018. Business model design: lessons learned from Tesla Motors. In: Towards a Sustainable Economy. Springer, pp. 53–69.

Chen, Z., Yin, Y., Song, Z., 2018. A cost-competitiveness analysis of charging infrastructure for electric bus operations. Transp. Res. C 93, 351–366.

Coelho, P., 2013. Linearization of the product of two variables. In: Canada Research Chair in Integrated Logistics.

Dafermos, S.C., Sparrow, F.T., 1969. The traffic assignment problem for a general network. J. Res. Nat. Bur. Stand. B 73 (2), 91–118.

Dey, M., Loewenstein, M.A., 2020. How many workers are employed in sectors directly affected by COVID-19 shutdowns, where do they work, and how much do they earn? Monthly Labor Rev. 1–19.

Ding, Y., Jian, S., 2022. Strategic collaboration between land owners and charging station operators: Lease or outsource? Transp. Res. B 166, 183–211.

Ding, Y., Li, S., Jian, S., 2022. Optimal pricing and fleet management for shared electric vehicle in coupled power and transport networks. Transp. Res. C 141, 103727.

Dong, J., Liu, C., Lin, Z., 2014. Charging infrastructure planning for promoting battery electric vehicles: An activity-based approach using multiday travel data. Transp. Res. C 38, 44–55.

Duvall, M., et al., 2004. Advanced batteries for electric-drive vehicles. Electr. Power Res. Inst. (EPRI).

Funke, S.Á., Sprei, F., Gnann, T., Plötz, P., 2019. How much charging infrastructure do electric vehicles need? A review of the evidence and international comparison. Transp. Res. D 77, 224–242.

He, Y., Liu, Z., Song, Z., 2022. Integrated charging infrastructure planning and charging scheduling for battery electric bus systems. Transp. Res. D 111, 103437.

He, J., Yang, H., Tang, T.-Q., Huang, H.-J., 2020. Optimal deployment of wireless charging lanes considering their adverse effect on road capacity. Transp. Res. C 111, 171–184.

He, F., Yin, Y., Zhou, J., 2013. Integrated pricing of roads and electricity enabled by wireless power transfer. Transp. Res. C 34, 1–15.

He, F., Yin, Y., Zhou, J., 2015. Deploying public charging stations for electric vehicles on urban road networks. Transp. Res. C 60, 227–240.

Hodgson, M.J., Rosing, K., Leontien, A., Storrier, G., 1996. Applying the flow-capturing location-allocation model to an authentic network: Edmonton, Canada. European J. Oper. Res. 90 (3), 427–443.

Iora, P., Tribioli, L., 2019. Effect of ambient temperature on electric vehicles' energy consumption and range: Model definition and sensitivity analysis based on nissan leaf data. World Electr. Veh. J. 10 (1), 2.

Jang, Y.J., 2018. Survey of the operation and system study on wireless charging electric vehicle systems. Transp. Res. C 95, 844–866.

Jang, Y.J., Jeong, S., Ko, Y.D., 2015. System optimization of the On-Line Electric Vehicle operating in a closed environment. Comput. Ind. Eng. 80, 222–235.

Jang, Y.J., Jeong, S., Lee, M.S., 2016. Initial energy logistics cost analysis for stationary, quasi-dynamic, and dynamic wireless charging public transportation systems. Energies 9 (7), 483.
Jeong, S., Jang, Y.J., Kum, D., 2015. Economic analysis of the dynamic charging electric vehicle. IEEE Trans. Power Electron. 30 (11), 6368–6377.
Kadri, A.A., Perrouault, R., Boujelben, M.K., Gicquel, C., 2020. A multi-stage stochastic integer programming approach for locating electric vehicle charging stations. Comput. Oper. Res. 117, 104888.
Kang, N., Feinberg, F.M., Papalambros, P.Y., 2015. Integrated decision making in electric vehicle and charging station location network design. J. Mech. Des. 137 (6), 061402.
Kapustin, N.O., Grushevenko, D.A., 2020. Long-term electric vehicles outlook and their potential impact on electric grid. Energy Policy 137, 111103.
Kchaou-Boujelben, M., 2021. Charging station location problem: A comprehensive review on models and solution approaches. Transp. Res. C 132, 103376.
Ko, Y.D., Jang, Y.J., Lee, M.S., 2015. The optimal economic design of the wireless powered intelligent transportation system using genetic algorithm considering nonlinear cost function. Comput. Ind. Eng. 89, 67–79.
Kundur, P., Paserba, J., Ajjarapu, V., Andersson, G., Bose, A., Canizares, C., Hatziargyriou, N., Hill, D., Stankovic, A., Taylor, C., et al., 2004. Definition and classification of power system stability IEEE/CIGRE joint task force on stability terms and definitions. IEEE Trans. Power Syst. 19 (3), 1387–1401.
Liu, H., Zou, Y., Chen, Y., Long, J., 2021. Optimal locations and electricity prices for dynamic wireless charging links of electric vehicles for sustainable transportation. Transp. Res. E 152, 102187.
Longo, M., Zaninelli, D., Viola, F., Romano, P., Miceli, R., Caruso, M., Pellitteri, F., 2016. Recharge stations: A review. In: 2016 Eleventh International Conference on Ecological Vehicles and Renewable Energies (EVER). IEEE, pp. 1–8.
Lukic, S., Pantic, Z., 2013. Cutting the cord: Static and dynamic inductive wireless charging of electric vehicles. IEEE Electrif. Mag. 1 (1), 57–64.
Maitra, A., Kook, K.S., Taylor, J., Giumento, A., 2010. Grid impacts of plug-in electric vehicles on Hydro Quebec's distribution system. In: IEEE PES T&D 2010. IEEE, pp. 1–7.
Manshadi, S.D., Khodayar, M.E., Abdelghany, K., Üster, H., 2017. Wireless charging of electric vehicles in electricity and transportation networks. IEEE Trans. Smart Grid 9 (5), 4503–4512.
Mubarak, M., Üster, H., Abdelghany, K., Khodayar, M., 2021. Strategic network design and analysis for in-motion wireless charging of electric vehicles. Transp. Res. E 145, 102179.
Muratori, M., Kontou, E., Eichman, J., 2019. Electricity rates for electric vehicle direct current fast charging in the United States. Renew. Sustain. Energy Rev. 113, 109235.
Narassimhan, E., Johnson, C., 2018. The role of demand-side incentives and charging infrastructure on plug-in electric vehicle adoption: analysis of US states. Environ. Res. Lett. 13 (7), 074032.
Ngo, H., Kumar, A., Mishra, S., 2020. Optimal positioning of dynamic wireless charging infrastructure in a road network for battery electric vehicles. Transp. Res. D 85, 102385.
Qin, J., Porter, J., Poolla, K., Varaiya, P., 2020. Piggyback on TNCs for electricity services: Spatial pricing and synergetic value. In: 2020 American Control Conference (ACC). IEEE, pp. 500–507.
Suomalainen, E., Colet, F., 2019. A corridor-based approach to estimating the costs of electric vehicle charging infrastructure on highways. World Electr. Veh. J. 10 (4), 68.
Tan, Z., Liu, F., Chan, H.K., Gao, H.O., 2022. Transportation systems management considering dynamic wireless charging electric vehicles: Review and prospects. Transp. Res. E 163, 102761.
Wang, X., Mackenzie, D., Zhou, Y., Ding, F., 2022. Predicted network equilibrium model of electric vehicles with stationary and dynamic charging infrastructure on the road network. IEEE Intell. Transp. Syst. Mag. 14 (2).
Wang, T., Yang, B., Chen, C., Guan, X., 2019. Wireless charging lane deployment in urban areas considering traffic light and regional energy supply-demand balance. In: 2019 IEEE 89th Vehicular Technology Conference (VTC2019-Spring). IEEE, pp. 1–5.
Wardrop, J.G., Whitehead, J.I., 1952. Correspondence. some theoretical aspects of road traffic research. Proc. Inst. Civ. Eng. 1 (5), 767–768.
Wu, F., Sioshansi, R., 2017. A stochastic flow-capturing model to optimize the location of fast-charging stations with uncertain electric vehicle flows. Transp. Res. D 53, 354–376.
Xie, F., Liu, C., Li, S., Lin, Z., Huang, Y., 2018. Long-term strategic planning of inter-city fast charging infrastructure for battery electric vehicles. Transp. Res. E 109, 261–276.
Zhang, H., Moura, S.J., Hu, Z., Song, Y., 2016. PEV fast-charging station siting and sizing on coupled transportation and power networks. IEEE Trans. Smart Grid 9 (4), 2595–2605.